

REVIEW ARTICLE

Open Access

Rare-earth based materials: an effective toolbox for brain imaging, therapy, monitoring and neuromodulation

Zheng Wei^{1,2}, Yawei Liu¹, Bo Li¹, Jingjing Li¹, Shuang Lu¹, Xiwen Xing³, Kai Liu^{1,2,4}, Fan Wang¹ and Hongjie Zhang^{1,2,4}

Abstract

Brain diseases, including tumors and neurodegenerative disorders, are among the most serious health problems. Non-invasively high-resolution imaging methods are required to gain anatomical structures and information of the brain. In addition, efficient diagnosis technology is also needed to treat brain disease. Rare-earth based materials possess unique optical properties, superior magnetism, and high X-ray absorption abilities, enabling high-resolution imaging of the brain through magnetic resonance imaging, computed tomography imaging, and fluorescence imaging technologies. In addition, rare-earth based materials can be used to detect, treat, and regulate of brain diseases through fine modulation of their structures and functions. Importantly, rare-earth based materials coupled with biomolecules such as antibodies, peptides, and drugs can overcome the blood-brain barrier and be used for targeted treatment. Herein, this review highlights the rational design and application of rare-earth based materials in brain imaging, therapy, monitoring, and neuromodulation. Furthermore, the development prospect of rare-earth based materials is briefly introduced.

Introduction


Brain diseases are globally challenging issues owing to the special lesion sites, complicated pathogenesis, high mortality, and poor prognosis^{1–4}. However, the complexity of the cerebral nerves, the limited regenerative capacity of brain tissues, and difficulty in delivering conventional drugs through the blood-brain barrier (BBB), severely restrict the diagnosis and treatment of brain diseases^{5,6}. Moreover, the brain is fragile, and minor disorders and trauma could lead to severe dysfunction. Therefore, the development of non-invasive, rapid, and

efficient visual diagnosis and treatment techniques is essential for understanding and treating brain diseases. Especially, the combination of imaging and therapy can greatly simplify the treatment process of brain diseases and reduce damage to brain tissue. Current methods of brain imaging, such as magnetic resonance imaging (MRI), fluorescence imaging and computed tomography (CT), are limited with biosafety, sensitivity, penetration depth, and resolution. In addition, craniotomy is usually required for brain treatment. Therefore, it is important to design new imaging and therapeutic agents to address brain diseases in a gentle and valid way.

Among the imaging and therapeutic agents, rare-earth based materials show great advantages and application prospects in brain imaging and brain diseases treatment due to their unique electrical, optical and magnetic properties^{7–10}. Materials doped with Gd³⁺, Ho³⁺ and Dy³⁺ ions possess high magnetic moment, high X-ray absorption coefficients and relatively long electron

Correspondence: Shuang Lu (slu@ciac.ac.cn) or Xiwen Xing (xingxiwen@jnu.edu.cn) or Fan Wang (wangfan@ciac.ac.cn)
¹State Key Laboratory of Rare Earth Resource Utilization, Changchun Institute of Applied Chemistry, Chinese Academy of Sciences, Changchun 130022, China
²School of Applied Chemistry and Engineering, University of Science and Technology of China, Hefei 230026, China
Full list of author information is available at the end of the article
These authors contributed equally: Zheng Wei, Yawei Liu

© The Author(s) 2022, corrected publication 2022

 **Open Access** This article is licensed under a Creative Commons Attribution 4.0 International License, which permits use, sharing, adaptation, distribution and reproduction in any medium or format, as long as you give appropriate credit to the original author(s) and the source, provide a link to the Creative Commons license, and indicate if changes were made. The images or other third party material in this article are included in the article's Creative Commons license, unless indicated otherwise in a credit line to the material. If material is not included in the article's Creative Commons license and your intended use is not permitted by statutory regulation or exceeds the permitted use, you will need to obtain permission directly from the copyright holder. To view a copy of this license, visit <http://creativecommons.org/licenses/by/4.0/>.

relaxation time^{11–13}, enabling high spatial resolution of T_1 -weighted, T_2 -weighted MRI and CT brain imaging. Moreover, the emission spectrum of the lanthanide (Ln) based materials could be modulated from ultraviolet (UV) region to near-infrared (NIR) region by excitation with NIR source, which could be used for down-conversion (DC) and upconversion luminescence (UCL) imaging¹⁴. Importantly, NIR light can prevent damage to normal tissues and avoid background fluorescence of biological systems, enabling brain imaging under the skull. Particularly, Ln^{3+} ions with different properties can be synthesized and doped into a single nanomaterial to realize multi-modal imaging, providing a powerful tool for high-quality imaging of the brain¹⁵. In addition to brain imaging, rare earth-based nanoparticles (RENPs) are available for image-guided synergistic therapy of brain diseases¹⁶. Various therapeutic strategies based on RENPs such as radiotherapy, photodynamic therapy (PDT) and photothermal therapy (PTT) have been extensively studied and reported^{17–21}. Moreover, by detecting the fluorescence changes, RENPs are also effective in monitoring neuronal activity, sensing ionic changes in the brain, and visualizing brain diseases^{22–24}. Furthermore, the RENPs-mediated wireless optogenetics technique is also developed for manipulating neural activity and treating neurological disorders²⁵. Importantly, the functionalization of RENPs can further improve their stability, biocompatibility, targeting ability and the ability to overcome the BBB^{26–29}. Therefore, the rare-earth based materials are expected to break through the current limitations of brain diseases imaging, therapy and early diagnosis.

Herein, the recent research in the preparation and application of rare earth-based diagnostic and therapeutic materials are summarized. We highlight four applications of rare-earth based materials, including brain imaging, brain diseases therapy, brain disease diagnosis and monitoring, and brain modulation through optogenetics (Fig. 1). The functional properties and structural design of rare-earth based materials are discussed in detail. The prospects and potential challenges of rare earth-based materials in brain-related clinical applications are also presented.

Rare-earth based materials for brain imaging

Magnetic resonance imaging

MRI has emerged as a safe, painless, and powerful diagnostic tool, which is widely used in brain imaging³⁰. High spatial resolution brain images are conducive to visualizing the mass lesions in brain tumors^{31,32}. In the process, contrast agents (CAs) are indispensable for obtaining high signal-to-noise ratio images³³. Among them, rare-earth based composites with superior optical and magnetic properties attract great attention due to their unique 4f external electronic structure. In particular,

Gd^{3+} ions can provide a high electron magnetic moment and effectively shorten the electron relaxation time because of the seven unpaired 4f electrons ($^8S_{7/2}$) and symmetrical ground state^{34,35}.

Currently, Gd-based complexes, for example, Gd-diethyltriampentacetate (Gd-DTPA), are used as clinical T_1 -weighted MRI contrast agents. They exhibited high sensitivity in monitoring BBB rupture, blood vessel, and hemodynamics³⁶. However, owing to the low longitudinal relaxivity ($r_1 = 3.5 \text{ mM}^{-1} \text{ s}^{-1}$) and short half-life (20 min), Gd-DTPA displayed poor selectivity to tissues and limited time-dependent brain imaging property³⁷. To address these problems, Li et al. embedded Gd-DTPA into Poly-N⁵-(3-hydroxypropyl)-L-glutamine (PHTG) chains to restrict rotational movement of Gd-DTPA moieties, and developed a new biodegradable nonionic polymeric CA, named PHTG-DTPA-Gd³⁸. It exhibited 3.7 times higher longitudinal relaxivity than Gd-DTPA. Notably, the terminal elimination half-life of PHTG-DTPA-Gd was extended to 8.4 h, allowing for long-term imaging. Benefiting from the long half-time and high r_1 value, cerebral vessels in mice could be imaged for 2 h with high resolution. Importantly, the PHTG-DTPA-Gd demonstrated superior biocompatibility and biodegradability due to their intrinsic nature. NaGdF_4 nanoparticles with high loading of Gd^{3+} are also effective MRI CAs. The longitudinal relaxation rate of NaGdF_4 is ($r_1 = 8.93 \text{ mM}^{-1} \text{ s}^{-1}$) about 2.3 times higher than that of conventional clinical CA ($r_1 = 3.8 \text{ mM}^{-1} \text{ s}^{-1}$)³⁹. Yao et al. used HIV-1 transactivator (TAT) peptides-modified NaGdF_4 (NaGdF_4 -TAT) to successfully track the fate of adoptive T-cells in an orthotopic glioblastoma bearing mice by T_1 -weighted MRI⁴⁰.

In addition to the short circulation lifetime in vivo, non-target specificity and poor BBB permeability are still challenging for the clinical applications of Gd-based CAs. To overcome these challenges, Li and coworkers designed a novel two-order targeted nanoprobe (Den-RGD-Angio)⁴¹. The fifth generation (G5) polyamide-amine (PAMAM) dendrimer was conjugated with DOTA moieties to chelate Gd^{3+} ions for high contrast MRI (Fig. 2a). Subsequently, cyclic (RGDyK) peptides and angiopep-2 peptides were grafted to the chain of PAMAM dendrimer to realize tumor targeting and effective penetration of BBB, respectively^{42,43}. Furthermore, the size of the Gd-based nanoparticles was proved to affect brain imaging quality⁴⁴. The high proportion of surface Gd^{3+} ions in ultra-small nanoparticles greatly induces the longitudinal relaxation of water protons through synergistic effect of Gd^{3+} ions, which improves the imaging contrast significantly (Fig. 2b)⁴⁵. Moreover, various strategies were applied to improve the biocompatibility of Gd-based CAs. Fortin et al. prepared one-pot PEG-coated Gd_2O_3 nanoparticles to improve the biocompatibility of Gd_2O_3

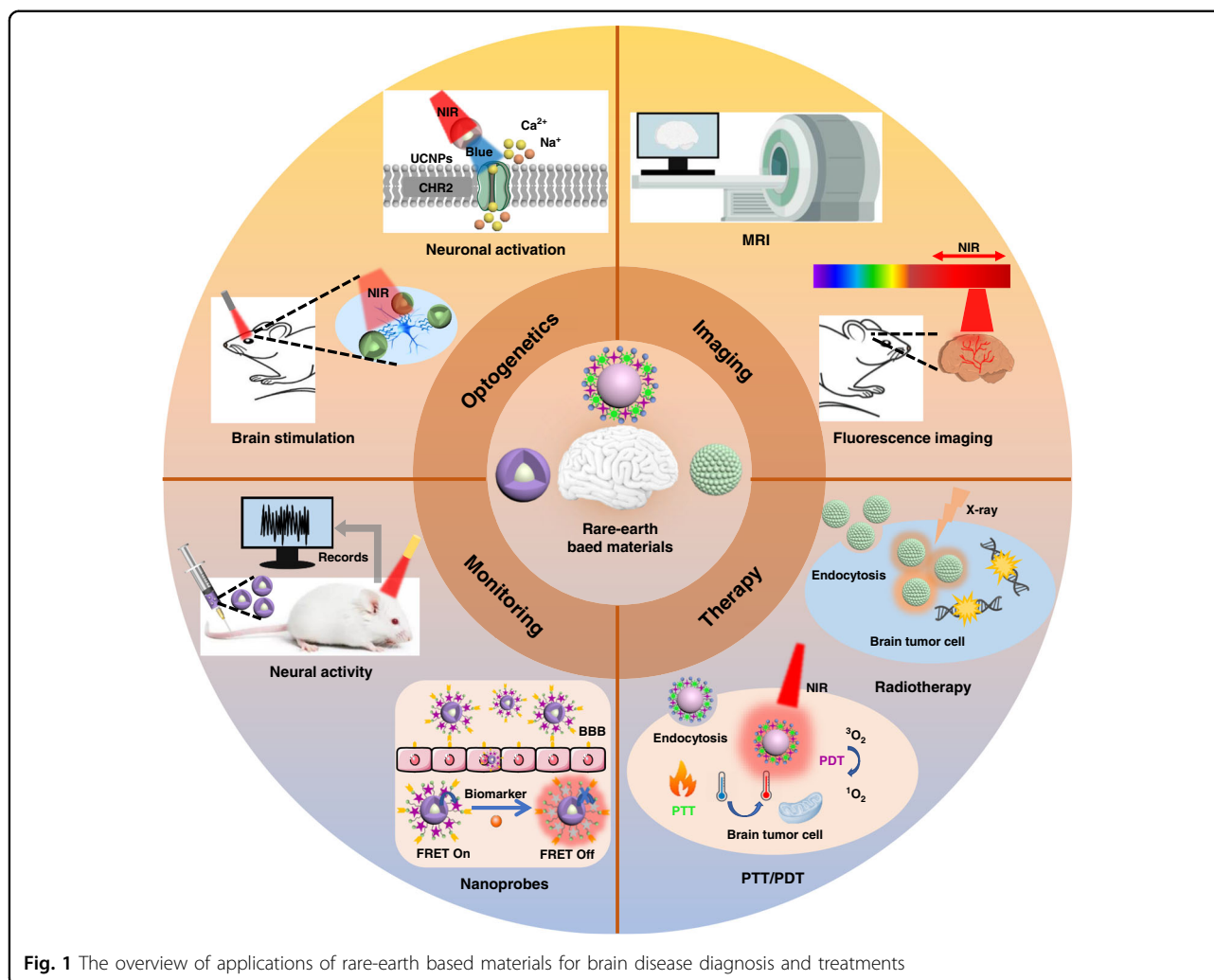


Fig. 1 The overview of applications of rare-earth based materials for brain disease diagnosis and treatments

nanoparticles⁴⁶. Chen et al. prepared poly (acrylic acid) (PAA)-stabilized Gd₂O₃ nanoparticles in aqueous phase and modified them with reduced bovine serum albumin (rBSA) to achieve good biocompatibility^{47–49}. Moreover, RGD dimer and lactoferrin (LF) were further covalently grafted to the Gd₂O₃ nanoparticle to achieve the BBB targeting and penetration. The achieved ES-GON-rBSA3-LF-RGD2 nanoparticles displayed an r_1 of 60.8 mM⁻¹ s⁻¹ at 1.5 T. After 12 h' injection of nanoparticles, the signal of T_1 -weighted MRI was enhanced to 423 ± 42%, which was 5–6 times higher than that of commercial Gd-based CAs (<80%), enabling high-contrast MRI of orthotopic glioblastoma (Fig. 2c).

Fluorescence imaging

Fluorescence imaging possesses the advantages of non-radiotoxicity, non-invasive, rapid detection, high sensitivity and superior imaging resolution^{50–52}. Over the past few decades, the fluorescence imaging mainly focused on

the visible region (400–700 nm) and NIR-I window (700–900 nm). However, photon scattering or photon absorption always occur when light enters tissue or bone, resulting in inevitable thermal damage, limited penetration depth and low signal-to-noise ratio⁵¹. Craniotomy, bone window opening and cranial grinding processes are usually required for traditional fluorescence imaging, further leading to damage to brain tissue and cerebral vessels⁵. The NIR-II (1000–1700 nm) fluorescence imaging technology is proved to have a higher spatial resolution, less thermal damage, deeper penetration depth and lower tissue autofluorescence. It can reach a depth of millimeters at sub-10 μm resolution to visualize the brain in real-time without the need for craniotomy⁵³. As promising nanomaterials for the next generation of in vivo fluorescence imaging, RENPs have superior photostability, long fluorescence lifetimes, narrow emission bandwidths and high biocompatibility^{14,54}. Particularly, their rich energy level transitions allow for the tunable

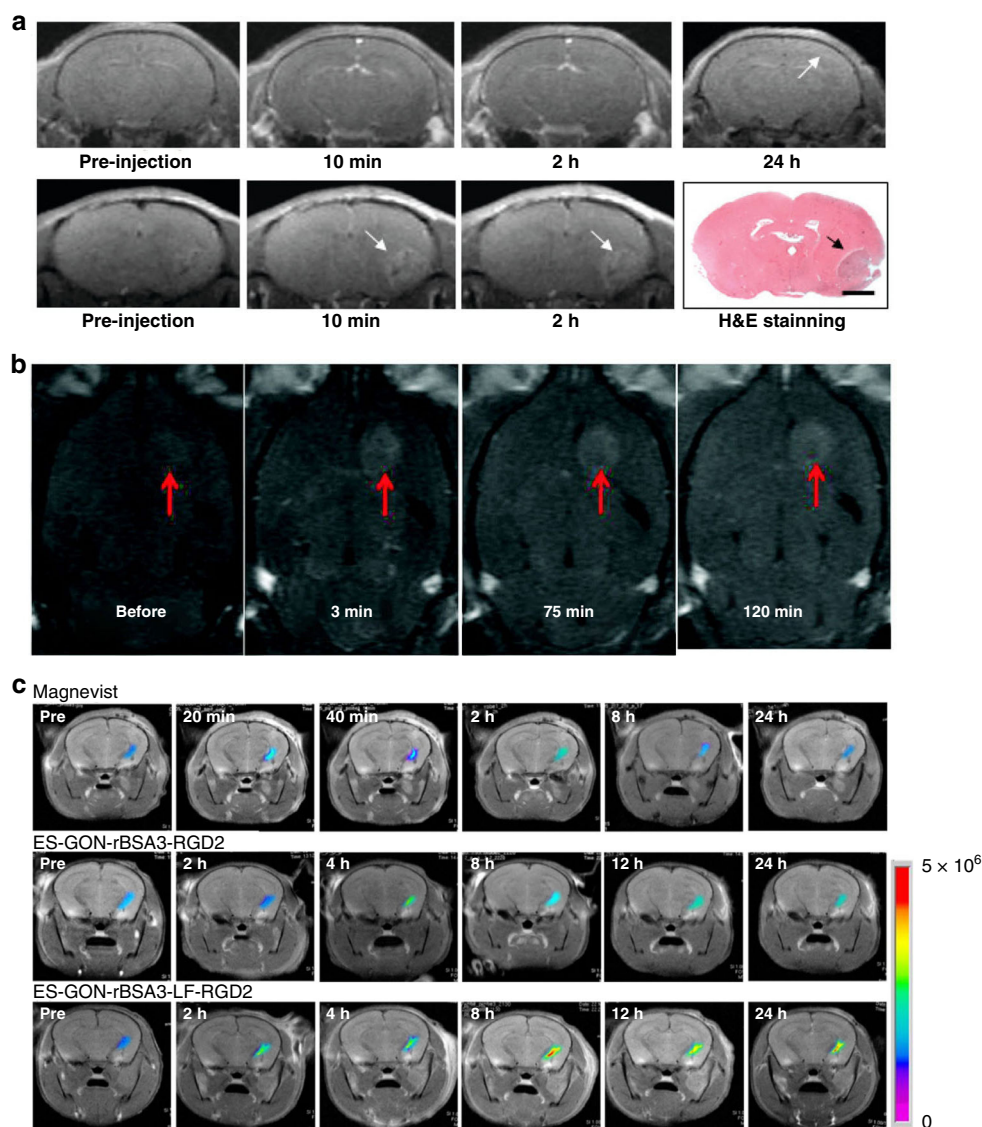


Fig. 2 In vivo brain MRI by using Gd-based CAs. **a** In vivo MRI of normal brain (top) and tumor-bearing brain (bottom) before and after injection of Den-RGD-Angio at different times. Reprinted with permission from ref. ⁴¹. Copyright 2012 American Chemical Society. **b** In vivo MRI of rat brain tumor after injection of ultra-small Gd_2O_3 nanoparticles. Reprinted with permission from ref. ⁴⁵. Copyright 2009 American Chemical Society. **c** In vivo MRI of tumor-bearing brain after injection of Magnevist, ES-GON-rBSA3-RGD2, and ES-GON-rBSA3-LF-RGD2 at different times. Reprinted with permission from ref. ⁴⁷. Copyright 2020 Elsevier

NIR-II emission by changing the doped ion species⁵⁰. Table 1 summarizes typical rare-earth based materials for NIR-II fluorescence imaging.

Er^{3+} -doped RENPs can emit luminescence at around 1500 nm, which are the most widely reported NIR-II imaging reagents. Dai's group reported a bright 1550 nm luminescent Er-based nanoparticle under 980 nm excitation⁵³. Ce^{3+} ions were co-doped into $NaYbF_4$ nanocrystal to suppress the upconversion process and promote 1550 nm emission by accelerating the effective photon-assisted nonradiative cross relaxation between Ce^{3+} ions

and Er^{3+} ions⁶⁶. Moreover, the inert $NaYF_4$ shell was applied to protect Er^{3+} ions from surface quenching⁶⁷. In addition, stability and biocompatibility were greatly enhanced by surface modification of amphiphilic polymer and PEG. Fast in vivo imaging of mice's cerebrovascular structure at a depth of 1.3 mm with an exposure time of only 20 ms was achieved by using this bright NIR-II fluorescent probe (Fig. 3a). Hao's group also fabricated the PAA-modified $NaLuF_4:Gd/Yb/Er/Ce$ nanorods for cerebrovascular imaging⁵⁵. The emission of RENPs beyond 1500 nm in an aqueous solution was enhanced by 1.75 to

Table 1 Typical rare-earth based materials for NIR-II fluorescence imaging

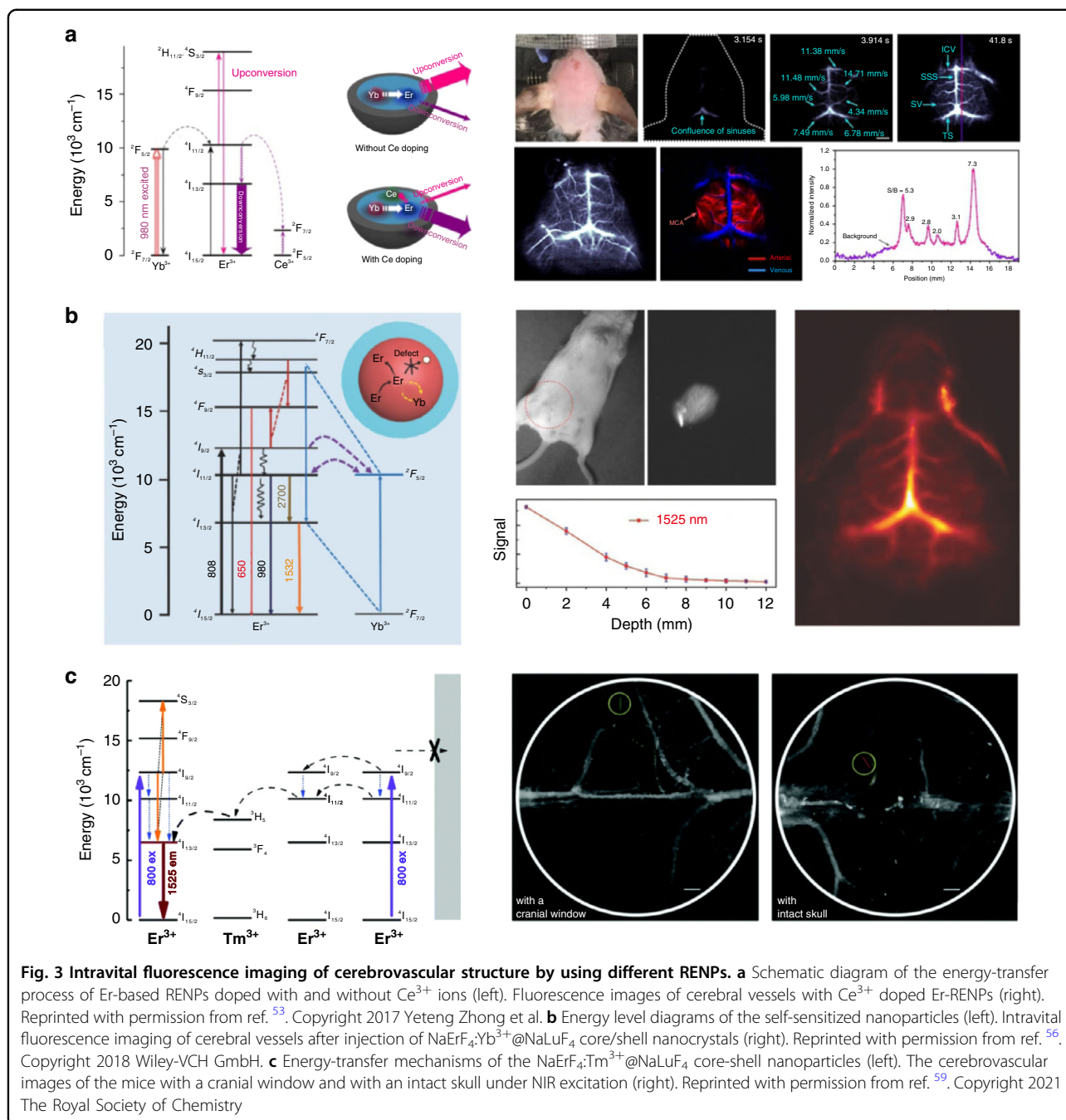
Rare-earth based materials	Excitation wavelength (nm)	Emission wavelength (nm)	NIR-II quantum yield (%)	Penetration depth (mm)	Year
NaYbF ₄ :Er/Ce @NaYF ₄	980	1550	2.73	>1.3 (under the intact scalp and skull)	2017 ⁵³
NaLnF ₄ :Gd/Yb /Er/Ce/nanorod	980	1525	3.6	–	2019 ⁵⁵
NaErF ₄ :Yb@ NaLuF ₄	808	1525	11	–	2018 ⁵⁶
Hexagonal-phase NaErF ₄ @NaYF ₄	808	1525	10.2	–	2020 ⁵⁷
NaYF ₄ :Yb:Nd@CaF ₂	800	1000	11	–	2018 ⁵⁸
NaErF ₄ :Tm@ NaLuF ₄	800	1525	13.92	–	2021 ⁵⁹
KSc ₂ F ₇ :Yb ³⁺ /Er ³⁺	980	1525	2.7	–	2018 ⁶⁰
NaNdF ₄ @NaLuF ₄ /IR-808	808	1060/1340	–	–	2019 ⁶¹
RENPs@Alk-Pi	808	1525	–	–	2021 ⁶²
NaErF ₄ :Ce@ NaYbF ₄ @NaLuF ₄ -Dye-BP	808	1525	–	>3	2020 ⁶³
QDs-LnNCs	975	1550	0.25	–	2021 ⁶⁴
Er(III)-bacteriochlorin complexes	760	1530	0.01(absolute quantum yield)	2 (in the hippocampus)	2021 ⁶⁵

2.2 times with co-doped with Ce³⁺ ions. Besides, the quantum yield of RENPs increased from 2.2% to 3.6% by replacing the NaYF₄ host with NaLuF₄ host. After 8 s injection of RENPs, the cerebral vessels of mice could be visualized clearly. Additionally, Chen's group reported a novel Er³⁺ self-sensitized core-shell NaErF₄:Yb³⁺@NaLuF₄ under 800 nm excitation⁵⁶. The inert shell of NaLuF₄ inhibited the luminescence concentration quenching and surface quenching, allowing 100% incorporation of Er³⁺ ions into the core. In addition, Yb³⁺ ions were doped as the energy trapping centers for enhancing NIR-II emission (Fig. 3b). The obtained RENPs possessed a high quantum yield of about 11%, enabling transcranial imaging of cerebral vessels in mice with an exposure time of 10 ms.

Furthermore, Chen's group investigated the influence of crystal phase, core-shell structure, shell matrix and shell thickness on the NIR-II emission of Er³⁺ self-sensitized nanoparticles⁵⁷. The brightest emission was obtained by hexagonal (β)-phase NaErF₄@NaYF₄ nanoparticles with an ultra-small size of 13 nm. Importantly, owing to the ultra-small size, these nanoparticles were completely excreted through feces in 14 days. Meanwhile, Liu et al. developed an efficient Er³⁺ self-sensitized system of NaErF₄:Tm³⁺@NaLuF₄⁵⁹. Tm³⁺ ions were introduced as the energy capture center and facilitated the energy transfer between Tm³⁺ ions and Er³⁺ ions. The obtained NaErF₄:Tm³⁺@NaLuF₄ nanoparticles exhibited a high quantum yield of 13.92%. After further modification with hydrophilic PEG, the nanoparticles achieved accurate NIR-II images of cerebral vessels with an intact skull

(Fig. 3c). In addition to the Ln-based host, a new orthorhombic Sc-based nanoprobe that co-doped with Yb³⁺/Er³⁺ was developed by Liu et al.⁶⁰. The Sc-based nanoprobe showed outstanding NIR-II luminescence at 1525 nm with a quantum yield of 2.7%, which could support non-invasive cerebrovascular visualization.

Although RENPs are desirable CAs for brain imaging, the absorption cross sections of the Ln³⁺ ions are extremely small, which impairs their performance in bio-imaging⁵⁴. The absorption cross sections of organic dyes are 10³–10⁴ times larger than Ln³⁺ ions, which can be employed as antennas to improve the light-harvesting capacity of Ln³⁺-based nanocrystals^{68–70}. Li et al. electrostatically anchored IR-808 molecules onto NaNdF₄@NaLuF₄ nanoparticles within a spatial distance of 2.4 nm, allowing the occurrence of Förster resonance energy transfer (FRET) from IR808 to Nd³⁺ ions⁶¹. By synergistically absorbing 808 nm light and efficiently transferring excited state energy, the NIR-II emission at 1060 nm and 1340 nm was significantly enhanced. The DSPE-PEG₅₀₀₀ was further coated to improve biocompatibility of nanoparticles. Finally, orthotopic glioblastoma was detected clearly by NIR-II fluorescence imaging with the focused ultrasound (FUS)-assisted technique⁷¹. In another work, Liu's group designed new NIR dyes to sensitize NaYF₄:Yb/Er@NaYF₄:Nd nanoparticles via the energy-transfer cascade: dye→Nd³⁺→Yb³⁺→Er³⁺ (Fig. 4a)⁶². They optimized the structure of NIR dyes by introducing long hydrophobic alkyl chains and electron-donating group. The as-obtained Alk-pi modified RENPs achieved a 40-fold enhancement of the NIR-II luminescence, providing



high-resolution NIR imaging of mice' brains without the need for craniotomy or skull thinning. To increase the stability of dye, Ren et al. designed a new dye-brush polymer (Dye-BP) and applied it on the surface of Er-based down-conversion nanoparticles (DCNPs) through ligand exchange processes⁶³. Through co-harvesting 808 nm photons by Dye-BP and transferring photons to $^4I_{9/2}$ energy level of Er^{3+} ions, the NIR-II emission of Er-DCNPs-Dye-BP was enhanced by 675-folds. Other materials with large absorption cross sections can also be

applied as an antenna to enhance the luminescent intensity of RENPs⁵⁴. The extinction coefficient of Ag₂Se quantum dots (QDs) is 2.8 L g⁻¹ cm⁻¹, which was 530 times higher than that of Yb-RENPs (5.2 × 10⁻³ L g⁻¹ cm⁻¹)^{64,72}. The Ag₂Se QDs sensitized RENPs possessed a 100-fold enhancement in the NIR-II luminescence intensity, enabling clear observation of dynamic cerebrovascular changes in traumatic brain injury (Fig. 4b). Inspired by the light-harvesting role of bacteriochlorin, Zhang et al. proposed a novel bacteriochlorin-sensitized

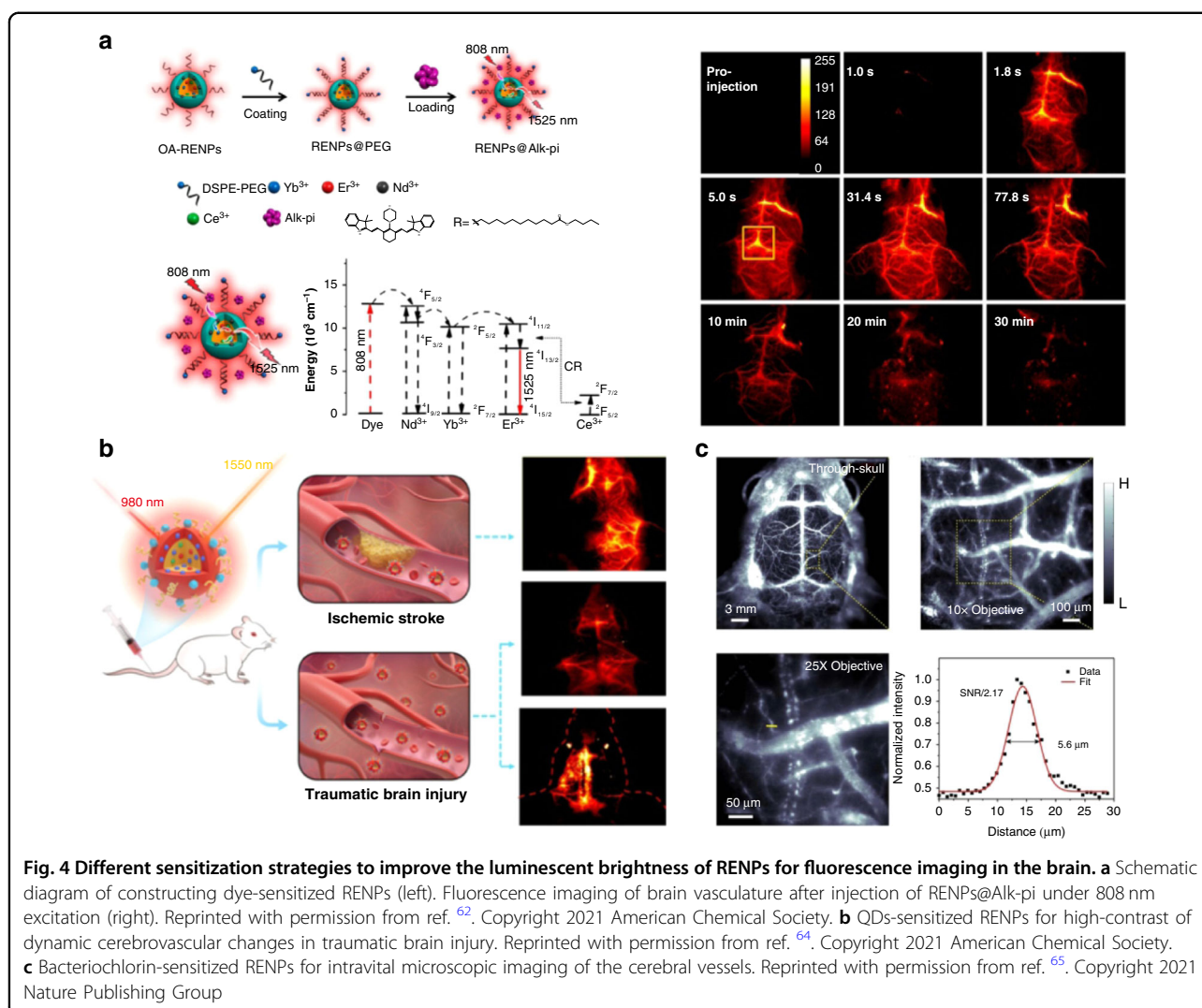


Fig. 4 Different sensitization strategies to improve the luminescent brightness of RENPs for fluorescence imaging in the brain. **a** Schematic diagram of constructing dye-sensitized RENPs (left). Fluorescence imaging of brain vasculature after injection of RENPs@Alk-pi under 808 nm excitation (right). Reprinted with permission from ref. ⁶². Copyright 2021 American Chemical Society. **b** QDs-sensitized RENPs for high-contrast of dynamic cerebrovascular changes in traumatic brain injury. Reprinted with permission from ref. ⁶⁴. Copyright 2021 American Chemical Society. **c** Bacteriochlorin-sensitized RENPs for intravital microscopic imaging of the cerebral vessels. Reprinted with permission from ref. ⁶⁵. Copyright 2021 Nature Publishing Group

NIR probe (EB766)⁶⁵. Bacteriochlorin acted as the antenna ligand to populate photons at the ⁴I_{13/2} level of Er³⁺ with an efficiency of about 99.9% and a rate constant of 2 × 10⁹ s⁻¹. BSA and cell-penetrating peptide HIV-TAT were further added to label the cancer cells for non-invasively monitoring their movement, migration, and residence in the cerebrovascular wall of the mouse through intravital NIR-II imaging (Fig. 4c).

Multi-modal imaging

MRI and fluorescence imaging are powerful tools for brain imaging. However, MRI displays poor spatial resolution, while fluorescence imaging has low fluorescence quantum yield⁷³. To address these shortcomings, multi-modal imaging was developed to provide more accurate imaging information of brain for further clinical applications. Notably, Ln³⁺ ions possess superior optical, magnetic properties, and high X-ray absorption coefficients (2.32–4.01 cm² g⁻¹), allowing for simultaneous MRI,

fluorescence imaging and CT imaging on a single material^{13,73,74}. For example, Wong's group integrated Gd³⁺-DOTA and NaYF₄:Yb/Er/Tm upconversion nanoparticles (UCNPs) for MR/ UCL dual-modal imaging of glioblastoma⁷⁵. The conjugated UCNP-Gd reagents displayed a high *r*₁ of 12.741 mM⁻¹ s⁻¹ at 300 MHz and strong UCL in deep-red region. RGD was further modified on the UCNP-Gd to specifically identify U87MG cells. As a result, the boundaries of glioblastoma could be delineated preoperatively and the resection of glioblastoma could be guided by the MRI/UCL imaging. Recently, Shi's group realized simultaneously MRI/fluorescence imaging on the single Gd-doped NaYF₄:Yb/Tm/Gd@NaGdF₄ nanoparticle (Fig. 5)⁷⁶. The introduction of Gd³⁺ ions provides high contrast MRI. Meanwhile, Tm³⁺ ions show strong UCL under 980 nm excitation. PEG and angiopep-2 peptide were then coupled onto NaYF₄:Yb/Tm/Gd@NaGdF₄ nanoparticles for water solubility and effective penetration of the BBB, respectively. These

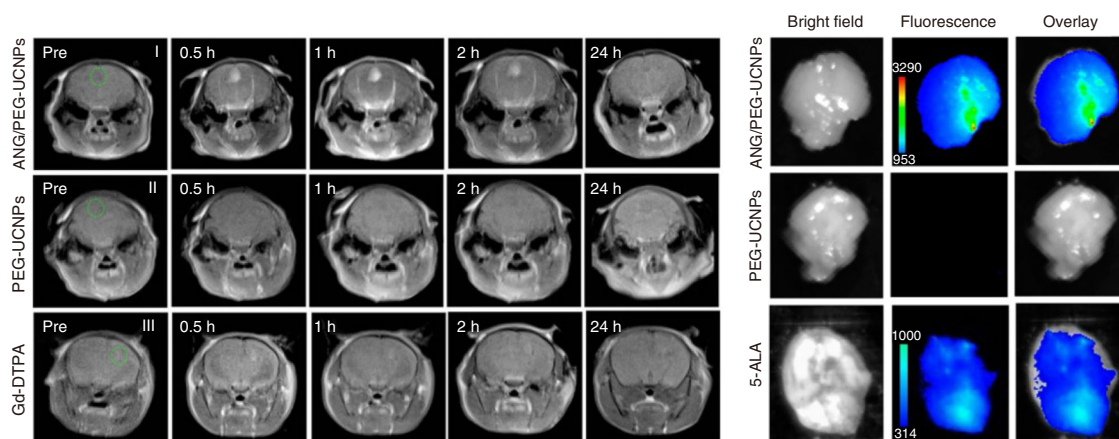


Fig. 5 Intravital dual-modal MRI/UCL imaging of brain tumor after injection of ANG/PEG-UCNPs, PEG-UCNPs and Gd-DTPA. Reprinted with permission from ref. ⁷⁶. Copyright 2014 American Chemical Society

nanoprobes achieved preoperative diagnosis and intraoperative localization of glioblastoma, which are better than the clinical MRI CA (Gd-DTPA) and fluorescent dye (5-ALA). In another exciting work, they prepared Ho^{3+} -doped NaYbF_4 UCNPs for tri-modal MRI/UCL/CT imaging⁷⁷. The short electronic transverse relaxation time and high effective magnetic moments of Ho^{3+} ions and Yb^{3+} ions made the UCNPs suitable for T_2 -weighted MRI^{12,35}. In addition, Ho^{3+} -based NaYbF_4 UCNPs could emit 540 nm light under 980 nm excitation, allowing for UCL imaging. Moreover, Ho^{3+} and Yb^{3+} ions possess high X-ray absorption coefficients, which are suitable for CT imaging. Therefore, MRI/UCL/CT tri-modal imaging could be achieved in single Ho^{3+} -based NaYbF_4 UCNPs. Additionally, Lu-based RENPs show the best CT imaging quality due to the high X-ray absorption coefficient of Lu^{3+} ions ($4.01 \text{ cm}^2 \text{ g}^{-1}$ at 100 keV). Zhou et al. prepared $\text{CsLu}_2\text{F}_7:\text{Yb}/\text{Er}/\text{Tm}$ -based nanoparticles for CT/UCL dual-modal imaging⁷⁸. Heavy alkali metal of Cs was used to replace Na in the UCNPs host lattice to provide enhanced CT signals. As a result, the dual-modal of CT and optical imaging realized real-time imaging and precise diagnosis of brain tumor.

Rare-earth based materials for brain disease therapy

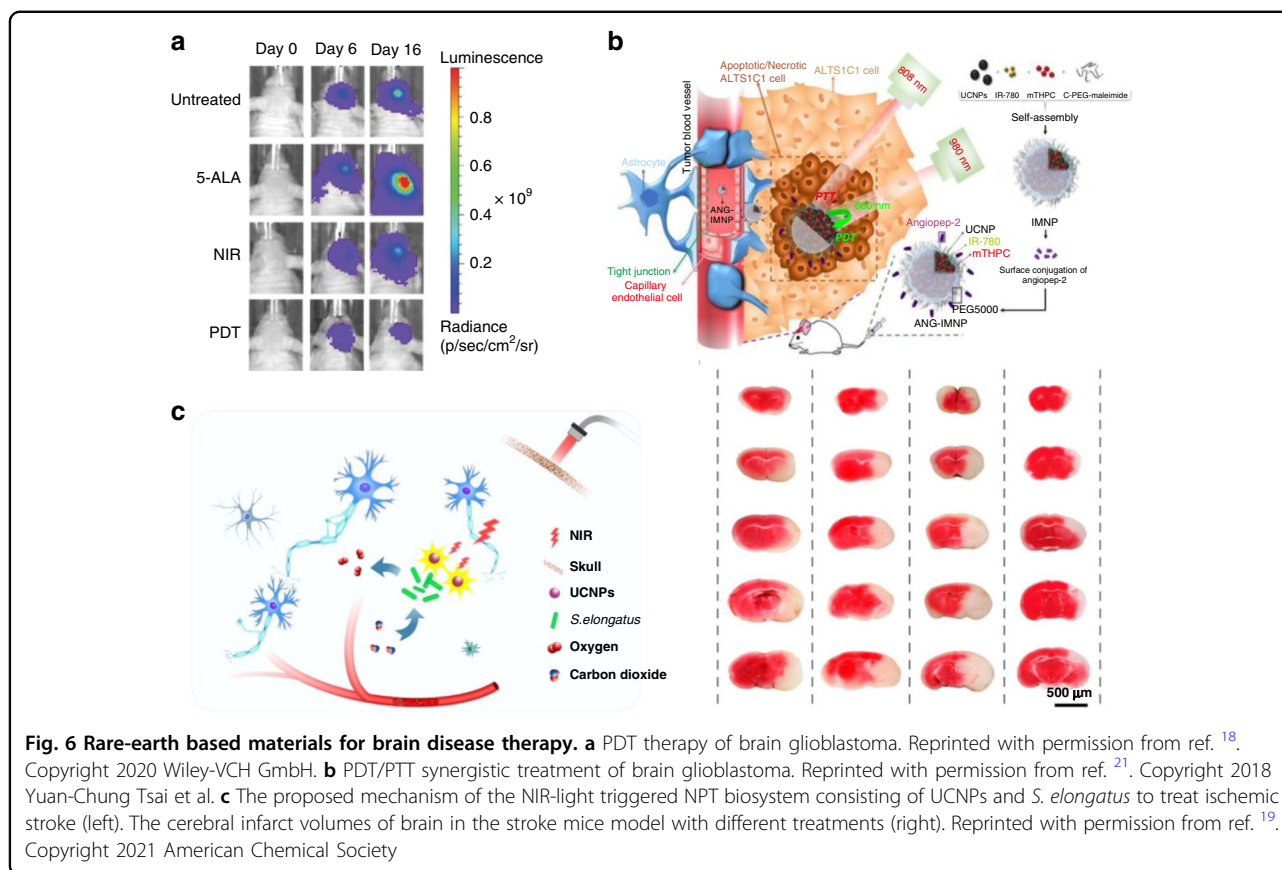
Radiotherapy

As the emerging multifunctional diagnostic and therapeutic agents, rare-earth based materials can be used not only for brain imaging but also for brain diseases therapy. Radiotherapy is a traditional treatment that uses radiation to locally kill tumors⁷⁹. However, radiotherapy is insensitive to the S-phase cells and hypoxic cells within the tumor. High radiation doses are always required to eliminate tumor cells, which inevitably cause damage to nearby normal tissues. Gd-based therapeutic agents with a

high X-ray absorption coefficient of $3.109 \text{ cm}^2 \text{ g}^{-1}$ are attractive agents for radiotherapy, which can increase the deposition of local radiation dose at the tumor site and significantly enhance the therapeutic effect⁴⁷. Olivier et al. proposed an imaging-guided radiotherapy through rapidly and precisely localizing Gd-based nanoparticles in the brain¹⁷. The superior MRI characteristics of Gd-based nanoparticles were used to monitor the real-time distribution of CAs in vivo. The irradiation only could be triggered when Gd-based nanoparticles were enriched in tumors, thereby significantly reducing the damage to surrounding healthy tissue. After 20 min of injection, more gadolinium was deposited in the diseased hemisphere, and the mice treated at this time displayed a long average survival time of 90 days.

Photodynamic therapy

PDT is a powerful way to treat diseases, which eliminates tumor by reactive oxygen species (ROS) generated through the reaction of photosensitizers with oxygen under the irradiation⁸⁰. Nevertheless, lots of photosensitizer molecules need to be excited by the UV or visible light that hardly penetrates the deep tissues and brain skeleton. The RENPs could emit tunable luminescence to sensitize the photosensitizers under NIR excitation, which greatly improve the penetration depth of PDT. Hyeon et al. assembled the photosensitizer Ce6 onto UCNPs via covalent conjugation and hydrophobic interaction for PDT treatment⁸¹. In this system, the red emission of UCNPs overlapped the absorption of Ce6, thereby inducing the PDT process under NIR excitation. In addition, UCNPs also acted as the carriers to deliver hydrophobic Ce6, which eliminates the aggregation of photosensitizers. Under 980 nm laser irradiation, the growth of U87MG tumor could be inhibited effectively. For enrichment of UCNPs at the tumor site along with



rapid clearance at the end of treatment, Kennedy's group designed an UCNP-based implant consisting of poly (ethylene glycol) diacrylate (PEGDA) core and fluorinated ethylene propylene (FEP) shell¹⁸. The photosensitizer precursor 5-ALA, which converted into the photosensitized metabolite protoporphyrin-IX (PpIX) in glioma cells, was pre-operatively injected to produce various ROS under the photoexcitation of implant^{82,83}. Under 980 nm laser irradiation, cellular mitochondria in tumor cells were damaged and eventually led to the death of tumor cells (Fig. 6a). Apart from brain tumors, other forms of brain diseases can be treated by PDT. C₆₀ molecule is a kind of functional photosensitizer molecule, which can jump to the triplet excitation state and generate ROS under UV or visible light. It can effectively scavenge ROS in the dark state owing to the huge unsaturated structure and superior electron affinity^{84,85}. Based on this photocontrolling mechanism, Qu et al. covalently linked C₆₀ and amyloid- β (A β) targeting peptides with UCNPs (UCNP@C₆₀-pep) to synergistically treat Alzheimer's disease (AD)²⁰. ROS generated by UCNP@C₆₀-pep could specifically oxidize A β and increase the hydrophilicity of A β , thereby significantly reducing the aggregation of oxidized A β . In dark conditions, UCNP@C₆₀-pep could scavenge overproduced ROS and maintain redox

homeostasis in vivo. The dual properties of UCNP@C₆₀-pep that either produce or scavenge ROS mitigated neurotoxicity, which could be used for alleviating A β -triggered paralysis and movement disorders.

Photothermal therapy

PTT is another phototherapeutic strategy, which employs photothermal materials to convert NIR laser into heat to treat disease^{86–89}. The high temperature can eliminate tumors by melting the membrane of tumor cells and denaturing proteins^{90,91}. Chiu et al. integrated the photothermal molecule and photosensitizer onto a single UCNP to achieve synergistic PTT and PDT treatment of glioblastoma (Fig. 6b)²¹. Cellular experiments demonstrated that synergistic therapy could effectively ablate 82% of tumor cells. The median survival time of mice receiving the synergistic therapy was significantly prolonged to 24 days, which was 3 times longer than the control group. In another work, Qu et al. proposed a NIR-light controlled microglia activation strategy for targeted therapy of brain diseases. They prepared mesoporous silica coated UCNP as drug loading platforms⁹². Photothermal agents indocyanine green (ICG) and microglia activator-bacterial lipopolysaccharide (LPS) were loaded into the pores of SiO₂. Subsequently, β -cyclodextrin (CD) and photoswitchable azobenzene (Azo)

were further capped on the surface to control the release of drugs. The heat generated by the loaded ICG under irradiation could induce the expression of heat shock proteins in microglia, which synergistically enhanced the activation effect from LPS. As a result, the secretion level of pro-inflammatory cytokine in microglia was effectively promoted under NIR irradiation.

Other therapies

In addition to radiotherapy, PDT and PTT, other new strategies have also been applied to synergistically treat brain disease with rare-earth based materials. Wang's group developed a NIR-light triggered nanophotosynthetic (NPT) biosystem consisting of core-shell Nd³⁺-doped UCNP and photoautotroph cyanobacterium (*S. elongatus*) to treat ischemic stroke (Fig. 6c)¹⁹. The depletion of oxygen as well as massive accumulation of carbon dioxide ultimately triggers irreversible neuronal damage. *S. elongatus* can spontaneously produce oxygen and consume carbon dioxide in the light. In vitro results showed that even in the presence of skull, UCNP could drive *S. elongatus* to produce more oxygen in the NIR light (170.0 mmHg) than under dark conditions (152.6 mmHg). Therefore, the NPT biosystem could effectively protect neurons from hypoxia-induced injury. The hypoxic area and cerebral infarction volume of NPT-treated mice were reduced by 60.2% and 51.6%, respectively. Notably, NPT could effectively improve motor coordination and promote poststroke angiogenesis in stroke mice.

Rare-earth based materials for early brain diseases monitoring and diagnosis

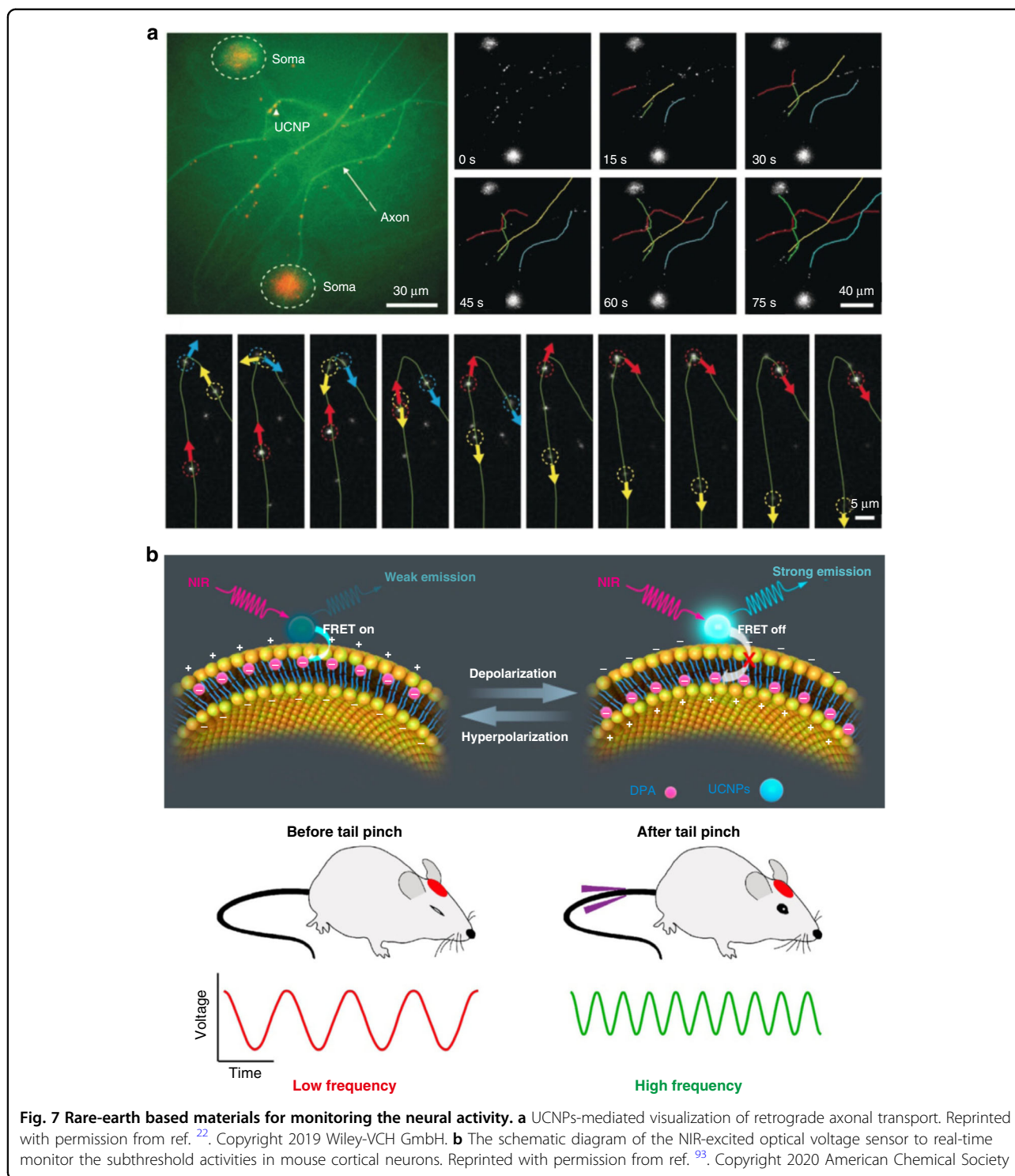
Monitor the neural activity

In addition to brain imaging and disease therapy, RENPs are promising candidates for monitoring brain neuronal activity and diagnosing brain diseases due to the superior luminescent properties. Monitoring neural activity, as well as neurological diseases, is conducive to understanding the pathogenesis and achieving an early diagnosis. Liu et al. used silica-coated NaLuF₄:Yb³⁺/Er³⁺ UCNP to realize real-time and continuous tracking of dynein movement inside neurons²². UCNP were endocytosed into the cell and trapped in the endosome. When the membrane receptors on the endosomes bound to cytoplasmic dynein via protein-protein interactions, the dynein would unidirectionally transport the endosomes containing UCNP to tens of micrometers away at a rate of 1–2 μm s⁻¹. The superior photostability allowed tracking the UCNP movement over 5 min without signal attenuation (Fig. 7a). Therefore, UCNP-mediated visualization of dynein-driven retrograde axonal transport provided insights into the mechanism of dynein movement, neurological disease pathology and the role of various neural circuits in the brain.

By utilizing FRET strategy between hexanitrodiphenylamine (DPA) and UCNP, Du's group designed a NIR-excited optical voltage sensor to real-time monitor the neuronal activity⁹³. As shown in Fig. 7b, UCNP and DPA were immobilized outside the cell membrane and inside the cell membrane, respectively. The absorption wavelength of DPA largely overlapped with the emission spectrum of UCNP, thus DPA could effectively quench the luminescence of the UCNP. However, the realization of energy transfer from UCNP to DPA required a close distance within 10 nm. The location of the negatively charged DPA was affected by the fluctuation of membrane potential, which influenced the distance between the DPA and UCNP, thereby causing the fluorescent changes of UCNP. Owing to the superior photostability of UCNP, the nanosensor could record the changes of the membrane potential with high fidelity for a long time. In addition, they showed the feasibility of the nanosensor for reporting neuronal activity in zebrafish and mice.

Detect the brain disease

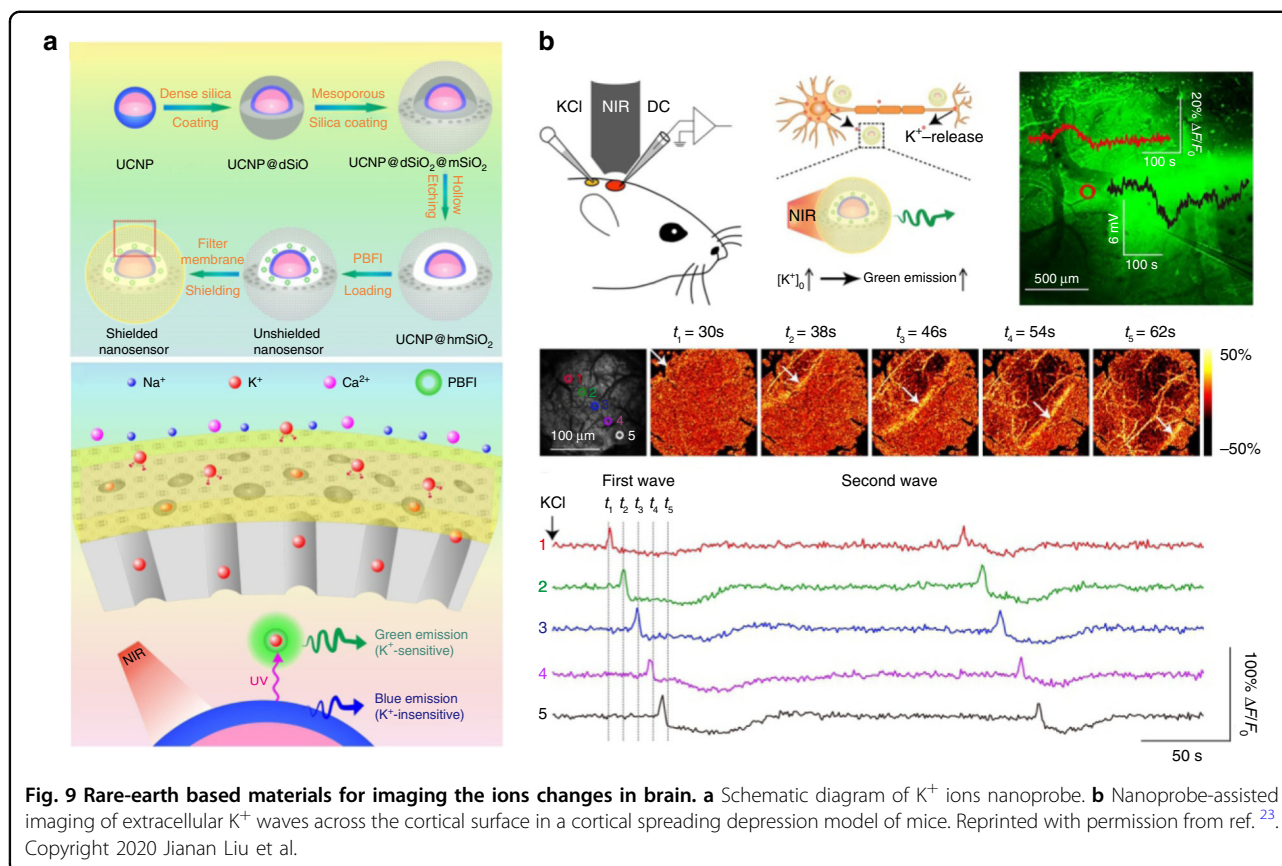
In addition to monitoring neural activity, rare-earth based nanoparticles can also be used to prepare fluorescent probes for detecting the brain diseases. Liu et al. designed HOCl-activated upconversion nanoprobe for visualizing neuroinflammation in vivo⁹⁴. Neuroinflammation is induced by activated microglia and astrocytes, accompanied by a substantial production of HOCl⁹⁵. As shown in Fig. 8a, Cy-HOCl dye was assembled with UCNP via hydrophobic interaction, which acted as energy receptor for UCNP and recognition unit of HOCl. The CyH-UCNP nanoprobe could detect HOCl in the LPS-induced neuroinflammation model through monitoring the luminescence intensity of UCNP. The luminescence intensity in the LPS-treated mice brain showed 1.8-fold enhancement compared with the control group, which suggested that overproduced HOCl could recover the luminescence of UCNP. After 10 min injection of nanoprobe, the intracerebral fluorescence signal intensity in mice with ischemic stroke was around 1.4 times higher than that in control groups, which enabled the real-time visualization of neuroinflammation. Meanwhile, Wong et al. designed the first Aβ oligomer-selective multimodal (MRI/NIR) contrast agent: NaGdF₄:Yb³⁺/Tm³⁺@NaGdF₄@SiO₂@F-SLOH and achieved detection and imaging of Aβ content in transgenic (Tg) AD mice of different age groups²⁴. The formation and deposition of Aβ oligomers are one of the biomarkers representing the early diagnosis of AD⁹⁶. The novel fluorine-substituted cyanine (F-SLOH) in nanosensor exhibited selectively binding affinity to Aβ oligomers and diverse response to different Aβ species⁹⁷. The fluorescence intensity of the nanosensor was different when they bounded with Aβ oligomers, Aβ monomers and fibrils. After



6 h injection of the nanosensor, the cerebrovascular fluorescence intensity of the transgenic AD mice demonstrated distinct age dependence. Older transgenic AD mice displayed a stronger fluorescence signal. Besides, the MRI signal of transgenic AD mice was generally stronger than that of wild-type (WT) mice (Fig. 8b).

Sensor the ions changes in brain

The ions changes are closely related to cell metabolism, apoptosis and neurotransmission⁹⁸. The sensor of the ions changes is beneficial for early detection of brain disease. By customized design of rare-earth based materials, the fluctuation of ions concentration in the brain can be



Rare-earth based materials for brain regulation through optogenetics

Optogenetics is an optical technique that uses visible light to activate channel proteins expressed in specific cells to remotely stimulate specific neurons deep in the brain¹⁰². The optogenetic stimulation of deep brain regions can induce multiple physiological phenomena including dopamine release, seizure inhibition, theta oscillation and memory recall, which could also be used for clinical treatment of neurological disorders¹⁰³. However, the visible light is strongly scattered in the tissues and cannot penetrate deep into brain. In addition, optical fibers are always required and invaded into brain for the optogenetics¹⁰⁴. UCNP can transform long-wavelength NIR light into diverse visible light, such as blue light, green light and so on. Benefiting from the unique upconverting fluorescent properties of UCNP, the UCNP-mediated optogenetics was proposed in 2011, which provides a minimally invasive technique that gets rid of the dependence on optical fibers, avoiding the damage to brain tissue caused by optical fibers¹⁰⁵. Table 2 lists the recent progress of rare-earth based materials-mediated optogenetics.

In proof-of-concept experiment, Yawo's group cultured C1V1 and *Platymonas subcordiformis* (PsChR)-expressing neurons on collagen-UCNP films¹⁰⁶. Then they

performed whole-cell patch-clamp experiments to prove the feasibility of NIR-mediated neuronal activity. The green emission of upconversion substrates under 980 nm irradiation could result in the inward photocurrents in C1V1-expressing neurons. Meanwhile, photocurrents were observed in PsChR-expressing cells when using blue-emitting UCNP-based membrane. Afterwards, Lee et al. prepared inorganic-organic hybrid nanomaterial scaffolds by encapsulating $NaYF_4:Yb^{3+}/Tm^{3+}@NaYF_4$ UCNP within the PLGA¹⁰⁷. The nanomaterials could emit blue light at 470 nm under 980 nm excitation, which could be used for activating channelrhodopsin-2 (ChR2). As shown in Fig. 10a, ChR2-expressing cells were cultured on the PLGA-UCNP hybrid scaffolds and displayed repetitive action potentials at frequencies up to 10 Hz under pulsed NIR light irradiation.

Although the in vitro optogenetics has been realized successfully, it's challenging to implant these large sized devices into the brain. In order to realize in vivo optogenetics, Shi's group packaged UCNP in a micro-optrode and made a fully implantable transducer device (Fig. 10b)¹¹¹. The small size of the UCNP-optrode ($\approx 100 \mu m$ in diameter, $< 1 mg$ in weight) enabled the simultaneous implantation of multiple UCNP-electrodes, which was conducive to achieving complex manipulation

Table 2 The recent progress of rare-earth based materials-mediated optogenetics

Biological model	Opsins	Absorption wavelength (nm)	Mode	Rare-earth based materials	Year
Cell	C1V1; PsCHR	549; 390–475	Activation	NaYF ₄ :Sc/Yb/Er; NaYF ₄ :Sc/Yb/Tm@NaYF ₄	2015 ¹⁰⁶
	Chr2	470	Activation	NaYF ₄ :Yb ³⁺ /Tm ³⁺ @NaYF ₄ poly(lactic-co-glycolic acid) scaffold	2015 ¹⁰⁷
	ReaChr	470–630	Activation	IR-806-β-NaYF ₄ :Yb ³⁺ /Er ³⁺ @β-NaYF ₄ :Yb/ poly(methyl methacrylate) matrix	2016 ¹⁰⁸
C. elegans	Chr2	475	Activation	NaYF ₄ :Yb ³⁺ /Tm ³⁺	2016 ¹⁰⁹
Zebrafish	Chr2	480	Activation	NaYF ₄ :Yb/Tm/Nd@NaYF ₄ :Nd	2017 ¹¹⁰
Mice	Chr2; C1V1	470; 540	Activation	NaYF ₄ :Yb/Tm@NaYF ₄ /glass micro-optrode; NaYF ₄ :Yb/Er@NaYF ₄ /glass micro-optrode	2017 ¹¹¹
	<i>eNpHR</i>	550	Inhibition	NaYF ₄ @NaYF ₄ :Yb/Er@NaYF ₄ /glass micro-optrode	2018 ¹¹²
	C1V1; ACR1	500-550	Activation; Inhibition	green-emitting lanthanide micro-particles;	2019 ¹¹³
	Chr2; Arch	475; 540	Activation; Inhibition	NaYF ₄ :Yb/Tm@SiO ₂ UCNP; NaYF ₄ :Yb/Er@SiO ₂ UCNP	2018 ¹⁰³

of brain activity with minor surgical lesions and inflammatory response. In their study, Tm³⁺-doped UCNP with the emission of 470 nm and Er³⁺-doped UCNP with the emission of 540 nm were sealed in micro-optrode to activate Chr2 and C1V1 opsins under 980 nm pulses, respectively. In addition, they designed a robotic system to automatically track animal's head. The combination of upconversion technology and robotic system could achieve effective transcranial nerve stimulation to various regions of the brain, which could be used for behavioral conditioning, locomotion pattern modulation and reflexive learning. For example, more contraversive turning in C1V1 mice ($4.68 \pm 0.26/\text{min}$) was induced than that in control groups ($1.48 \pm 0.17/\text{min}$) upon NIR irradiation. Furthermore, they encapsulated core-shell-shell UCNP with emission wavelength around 550 nm in glass micro-optrode to activate enhanced natronomonas halorhodopsin (*eNpHR*) opsin protein for neuronal inhibition¹¹². When this UCNP-based glass micro-optrode was implanted in the rat brain, the neuronal activity was inhibited under NIR irradiation. The system was further applied to perform tetherless deep brain inhibition in freely moving mice. As a result, the total movement distance of the mice was significantly reduced by 49.5%.

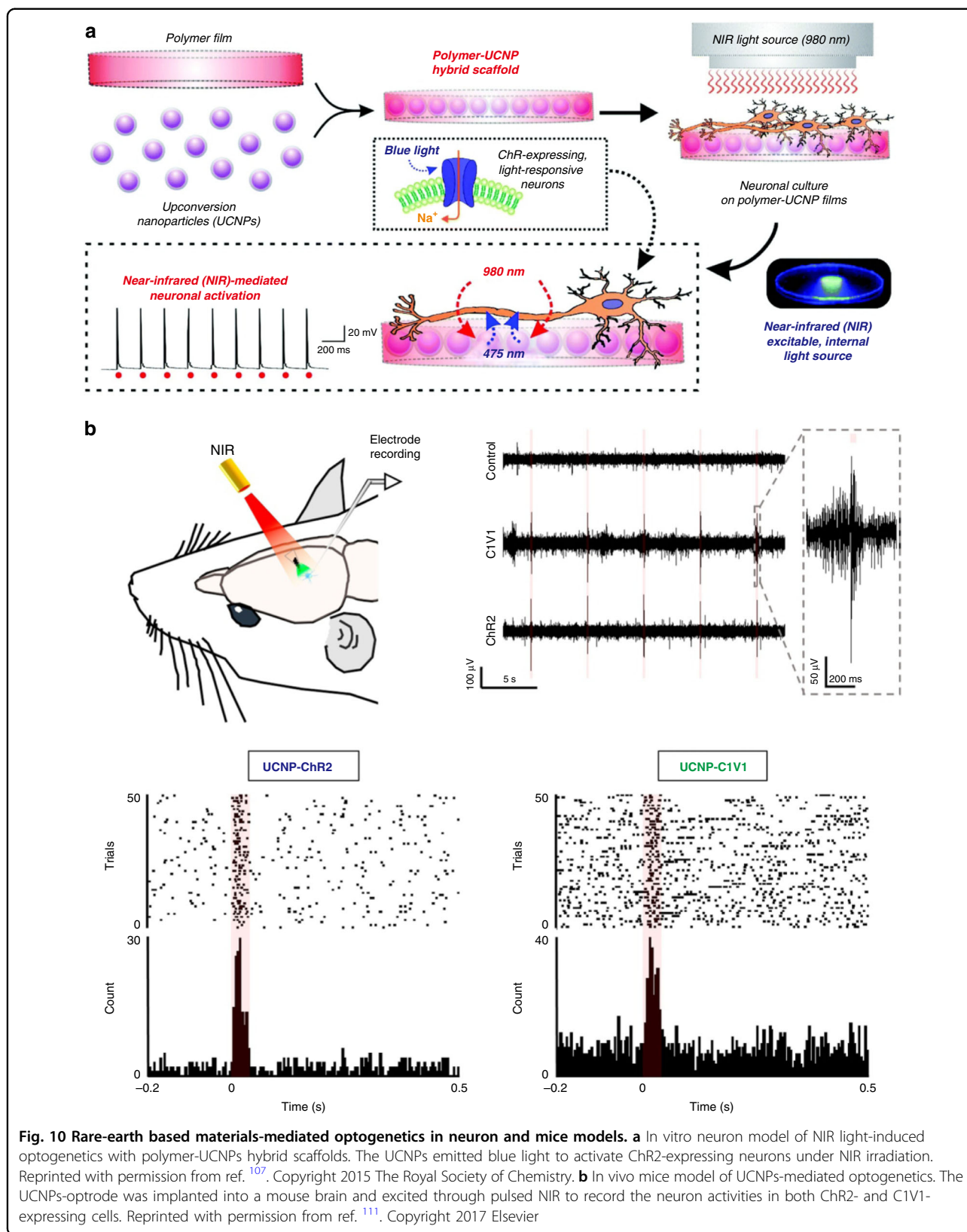
To reduce the brain injury caused by implanting devices, McHugh et al. developed minimally invasive “fiberless” optogenetics technique based on UCNP¹⁰³. Blue-emitting UCNP were injected near dopamine neurons in the ventral tegmental area (VTA) of mice to manipulate the release of dopamine (Fig. 11a). In addition, green-emitting UCNP were also injected in the hippocampus of mice to silence seizure (Fig. 11b). The above processes could be activated

under NIR irradiation transcranially. Furthermore, they employed transcranial NIR UCNP-mediated optogenetics to stimulate hippocampal granule cells that related to memory recall, and fear memory in mice could be successfully evoked even two weeks after injection of UCNP (Fig. 11c).

Conclusions and outlook

Rare-earth based materials with superior magnetism, unique optical properties, and high X-ray absorption coefficients are superior CAs for MRI, fluorescence imaging, and CT imaging. Notably, the multi-modal imaging based on a single rare-earth based material is also realized, providing more accurate and comprehensive information about brain. Moreover, rare-earth based materials are also effective in the treatment of brain diseases. Radiotherapy, PDT and PTT are applied to treat brain tumors. Luminescent RENPs-based probes are used for early brain diseases diagnosis. UCNP-mediated wireless optogenetic technique is developed for complex manipulation of brain activity with minor surgical lesions and inflammatory response. In conclusion, rare-earth based materials exhibit bright prospects in the field of integrated diagnosis and therapy. With the continual advancements of synthesis method coupled with the instrument technology, the development of rare-earth based materials for clinical brain disease treatment is highly promising. However, challenges remain in the development of rare-earth based materials:

(1) The fluorescence quantum yield and fluorescence intensity of the RENPs in aqueous solution is still very low. The development of highly robust synthetic methods and efficient structural modulation strategies is required to enhance the optical performance of RENPs.



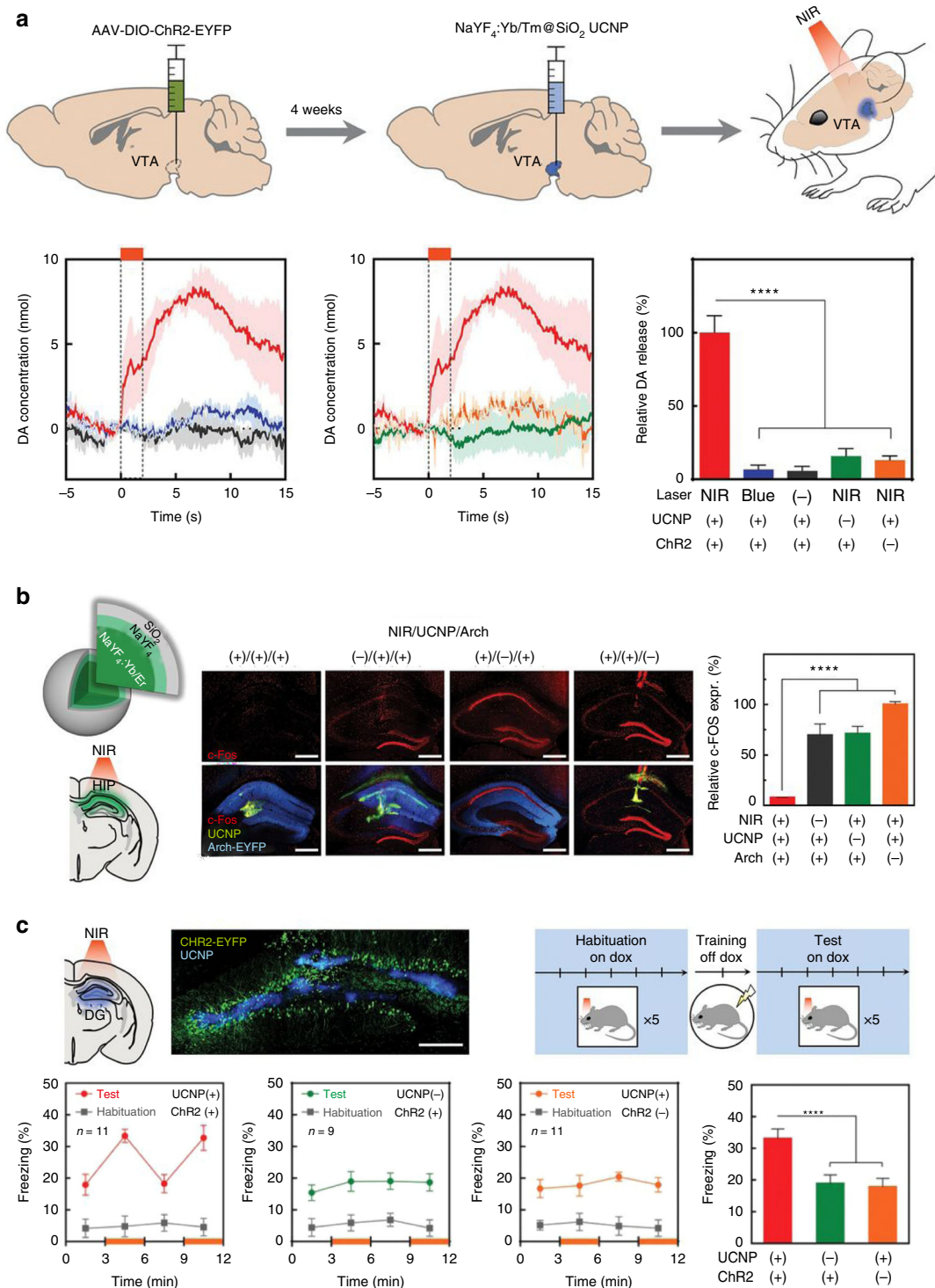


Fig. 11 NIR deep-brain stimulation through UCNPs-mediated optogenetics. **a** Transcranial NIR stimulation of VTA dopamine neurons. In the presence of both UCNPs and ChR2, significant release of dopamine can be detected under the stimulation of NIR. **b** Transcranial NIR inhibition of neural activity to silence seizure. **c** Transcranial NIR stimulation of hippocampal engram for memory recall. Reprinted with permission from ref. 103. Copyright 2018 American Association for the Advancement of Science

(2) Most of the reported RENPs are activated by NIR-I region, resulting in inevitable partial consumption of excitation light. Therefore, the development of RENPs with excitation wavelengths located in the NIR-II region is required to obtain clearer and more precise images. In addition, other Ln³⁺ doped RENPs, such as Ho³⁺ and Pr³⁺, are also need to be explored to broaden the available imaging agents.

(3) Overall, NIR-II biomedical fluorescence imaging based on RENPs is still in its infancy. In addition to low fluorescence quantum yield of rare-earth based materials, the lack of high-quality and low-cost charge-coupled device (CCD) detectors is also a major obstacle for NIR-II biomedical luminescence imaging. In addition, the combination setup of NIR-II fluorescence imaging strategy and other imaging strategy is immature and limited until now. The development of longer wavelength fluorescent probes and imaging instruments is urgently required, which will promote the further expansion of multi-modal imaging technology based on the NIR-II region.

(4) Non-invasive delivery of RENPs across the BBB is still a challenge. Currently, focused ultrasound (FUS) assisted technique that harmful to brain is still used to delivery drugs crossing the BBB. Therefore, other BBB-crossing methods including cell penetrating peptide/cells mediated brain delivery and receptor-mediated BBB opening need to be further explored¹¹⁴.

(5) Existing clinical CAs still meet the risk of releasing free rare earth ions in complex physiological environment during brain imaging process. In addition, the clearance of RENPs in body also needs to be considered. Thus, it is necessary to develop effective synthesis and assembly strategies to improve the stability, biocompatibility and in vivo clearance of rare-earth based materials.

(6) The technical challenge of implanting UCNPs into the specific deep brain regions with minimal invasion or noninvasion still exists for NIR-activated transcranial optogenetics. The UCNPs are injected stereotactically nowadays, which may cause damage to the brain. Thus, seeking new approaches to deliver UCNPs noninvasively to the specific neurons is urgently needed.

Acknowledgements

This research was supported by the National Key R&D Program of China (2020YFA0908900, 2021YFB3502300, and 2020YFA0712102), National Natural Science Foundation of China (Grant No. 21834007, 22020102003, 22107097, 21907088, and 22125701), Youth Innovation Promotion Association of CAS (Grant No. 2020228, 2021226) and China Postdoctoral Science Foundation (2020M681055).

Author details

¹State Key Laboratory of Rare Earth Resource Utilization, Changchun Institute of Applied Chemistry, Chinese Academy of Sciences, Changchun 130022, China. ²School of Applied Chemistry and Engineering, University of Science and Technology of China, Hefei 230026, China. ³Department of Biotechnology, College of Life Science and Technology, Jinan University, Guangzhou 510632, China. ⁴Department of Chemistry, Tsinghua University, Beijing 100084, China

Conflict of interest

The authors declare no competing interests.

Received: 25 February 2022 Revised: 13 May 2022 Accepted: 25 May 2022

Published online: 10 June 2022

References

- Fan, J., Dawson, T. M. & Dawson, V. L. Cell death mechanisms of neurodegeneration. In *Neurodegenerative Diseases: Pathology, Mechanisms, and Potential Therapeutic Targets* (eds Beart, P. H. et al.), 403–425 (Cham: Springer, 2017).
- Hardy, J. Neurodegeneration: the first mechanistic therapy and other progress in 2017. *Lancet Neurol.* **17**, 3–5 (2018).
- Sampson, J. H., Maus, M. V. & June, C. H. Immunotherapy for brain tumors. *J. Clin. Oncol.* **35**, 2450–2456 (2017).
- Ren, Y. B. et al. Highly reliable and efficient encoding systems for hexadecimal polypeptide-based data storage. *Fundament. Res.* <https://doi.org/10.1016/j.fjmr.2021.11.030> (2021).
- Wang, H. et al. Brain imaging with near-infrared fluorophores. *Coord. Chem. Rev.* **380**, 550–571 (2019).
- Wang, S. D. et al. Improving bioavailability of hydrophobic prodrugs through supramolecular nanocarriers based on recombinant proteins for osteosarcoma treatment. *Angew. Chem. Int. Ed.* **60**, 11252–11256 (2021).
- Qu, Z. B. et al. Near-IR emissive rare-earth nanoparticles for guided surgery. *Theranostics* **10**, 2631–2644 (2020).
- Liu, Y. W. et al. Highly plasticized lanthanide luminescence for information storage and encryption applications. *Adv. Sci.* **9**, 2105108, <https://doi.org/10.1002/advs.202105108> (2022).
- Wan, S. K. et al. A library of thermotropic liquid crystals of inorganic nanoparticles and extraordinary performances based on their collective ordering. *Nano Today* **38**, 101115 (2021).
- Shao, B. Q. et al. Engineered anisotropic fluids of rare-earth nanomaterials. *Angew. Chem. Int. Ed.* **59**, 18213–18217 (2020).
- Cao, Y. et al. Gadolinium-based nanoscale MRI contrast agents for tumor imaging. *J. Mater. Chem. B* **5**, 3431–3461 (2017).
- Viswanathan, S. et al. Alternatives to gadolinium-based metal chelates for magnetic resonance imaging. *Chem. Rev.* **110**, 2960–3018 (2010).
- Liu, Y. L. et al. A high-performance ytterbium-based nanoparticulate contrast agent for in vivo X-Ray computed tomography imaging. *Angew. Chem. Int. Ed.* **51**, 1437–1442 (2012).
- Zhong, Y. T. & Dai, H. J. A mini-review on rare-earth down-conversion nanoparticles for NIR-II imaging of biological systems. *Nano Res.* **13**, 1281–1294 (2020).
- Escudero, A. et al. Rare earth based nanostructured materials: synthesis, functionalization, properties and bioimaging and biosensing applications. *Nanophotonics* **6**, 881–921 (2017).
- Cai, X. L. et al. Photothermal-activatable liposome carrying tissue plasminogen activator for photoacoustic image-guided ischemic stroke treatment. *Small Struct.* **3**, 2100118 (2022).
- Le Duc, G. et al. Toward an image-guided microbeam radiation therapy using gadolinium-based nanoparticles. *ACS Nano* **5**, 9566–9574 (2011).
- Teh, D. B. L. et al. A Flexi-PEGDA upconversion implant for wireless brain photodynamic therapy. *Adv. Mater.* **32**, 2001459 (2020).
- Wang, J. et al. Oxygen-generating cyanobacteria powered by upconversion-nanoparticles-converted near-infrared light for ischemic stroke treatment. *Nano Lett.* **21**, 4654–4665 (2021).
- Du, Z. et al. Near-infrared switchable fullerene-based synergy therapy for Alzheimer's disease. *Small* **14**, 1801852 (2018).
- Tsai, Y. C. et al. Targeted delivery of functionalized upconversion nanoparticles for externally triggered photothermal/photodynamic therapies of brain glioblastoma. *Theranostics* **8**, 1435–1448 (2018).
- Zeng, X. et al. Visualization of intra-neuronal motor protein transport through upconversion microscopy. *Angew. Chem. Int. Ed.* **58**, 9262–9268 (2019).
- Liu, J. N. et al. A highly sensitive and selective nanosensor for near-infrared potassium imaging. *Sci. Adv.* **6**, eaax9757 (2020).
- Wang, C. K. et al. Amyloid- β oligomer-targeted gadolinium-based NIR/MR dual-modal theranostic nanoprobe for Alzheimer's disease. *Adv. Funct. Mater.* **30**, 1909529 (2020).

25. All, A. H. et al. Expanding the toolbox of upconversion nanoparticles for in vivo optogenetics and neuromodulation. *Adv. Mater.* **31**, 1803474 (2019).
26. Meng, Z. J. et al. Highly stiff and stretchable DNA liquid crystalline organogels with super plasticity, ultrafast self-healing, and magnetic response behaviors. *Adv. Mater.* **34**, 2106208 (2022).
27. Thanh, N. T. K. & Green, L. A. W. Functionalisation of nanoparticles for biomedical applications. *Nano Today* **5**, 213–230 (2010).
28. Wang, S. D. et al. Knockdown of a specific circular non-coding RNA significantly suppresses osteosarcoma progression. *Engineering*. <https://doi.org/10.1016/j.eng.2021.12.007> (2022).
29. Huang, J. Y. et al. Arranging small molecules with subnanometer precision on DNA origami substrates for the single-molecule investigation of protein–ligand interactions. *Small Struct.* **1**, 2000038 (2020).
30. Weber, M. A., Giesel, F. L. & Stieltjes, B. MRI for identification of progression in brain tumors: from morphology to function. *Expert Rev. Neurotherapeutics* **8**, 1507–1525 (2008).
31. Knopp, E. A. et al. Glial neoplasms: dynamic contrast-enhanced T₂*-weighted MR imaging. *Radiology* **211**, 791–798 (1999).
32. Knopp, M. V. et al. Primary and secondary brain tumors at MR imaging: bicentric intraindividual crossover comparison of gadobenate dimeglumine and gadopentetate dimeglumine. *Radiology* **230**, 55–64 (2004).
33. Caravan, P. et al. Gadolinium(III) chelates as MRI contrast agents: structure, dynamics, and applications. *Chem. Rev.* **99**, 2293–2352 (1999).
34. Binnemans, K. Lanthanide-based luminescent hybrid materials. *Chem. Rev.* **109**, 4283–4374 (2009).
35. Kattel, K. et al. A facile synthesis, in vitro and in vivo MR studies of D-glucuronic acid-coated ultrasmall Ln₂O₃ (Ln = Eu, Gd, Dy, Ho, and Er) nanoparticles as a new potential MRI contrast agent. *ACS Appl. Mater. Interfaces* **3**, 3325–3334 (2011).
36. Giesel, F. L., Mehndiratta, A. & Essig, M. High-relaxivity contrast-enhanced magnetic resonance neuroimaging: a review. *Eur. Radiol.* **20**, 2461–2474 (2010).
37. Weinmann, H. J. et al. Characteristics of gadolinium-DTPA complex: a potential NMR contrast agent. *Am. J. Roentgenol.* **142**, 619–624 (1984).
38. Zhang, G. D. et al. The degradation and clearance of Poly(N-hydroxypropyl-L-glutamine)-DTPA-Gd as a blood pool MRI contrast agent. *Biomaterials* **33**, 5376–5383 (2012).
39. Xing, H. Y. et al. Ultrasmall NaGdF₄ nanodots for efficient MR angiography and atherosclerotic plaque imaging. *Adv. Mater.* **26**, 3867–3872 (2014).
40. Zhang, H. et al. In vivo MR imaging of glioma recruitment of adoptive T-cells labeled with NaGdF₄-TAT nanoparticles. *Small* **14**, 1702951 (2018).
41. Yan, H. H. et al. Two-order targeted brain tumor imaging by using an optical/paramagnetic nanoprobe across the Blood Brain Barrier. *ACS Nano* **6**, 410–420 (2012).
42. Schottelius, M. et al. Ligands for mapping α_vβ₃-integrin expression in vivo. *Acc. Chem. Res.* **42**, 969–980 (2009).
43. Maletínská, L. et al. Human glioblastoma cell lines: levels of low-density lipoprotein receptor and low-density lipoprotein receptor-related protein. *Cancer Res.* **60**, 2300–2303 (2000).
44. Faucher, L. et al. Ultra-small gadolinium oxide nanoparticles to image brain cancer cells in vivo with MRI. *Contrast Media Mol. Imaging* **6**, 209–218 (2010).
45. Park, J. Y. et al. Paramagnetic ultrasmall gadolinium oxide nanoparticles as advanced T₁ MRI contrast agent: account for large longitudinal relaxivity, optimal particle diameter, and in vivo T₁ MR images. *ACS Nano* **3**, 3663–3669 (2009).
46. Faucher, L. et al. Rapid synthesis of PEGylated ultrasmall gadolinium oxide nanoparticles for cell labeling and tracking with MRI. *ACS Appl. Mater. Interfaces* **4**, 4506–4515 (2012).
47. Shen, Z. Y. et al. Small-sized gadolinium oxide based nanoparticles for high-efficiency theranostics of orthotopic glioblastoma. *Biomaterials* **235**, 119783 (2020).
48. Sun, J. et al. Mechanically strong proteinaceous fibers: engineered fabrication by microfluidics. *Engineering* **7**, 615–623 (2021).
49. Xiao, L. L. et al. An artificial phase-transitional underwater biogel with robust and switchable adhesion performance. *Angew. Chem. Int. Ed.* **60**, 12082–12089 (2021).
50. Fan, Y. & Zhang, F. A new generation of NIR-II probes: lanthanide-based nanocrystals for bioimaging and biosensing. *Adv. Optical Mater.* **7**, 1801417 (2019).
51. Hong, G. S., Antaris, A. L. & Dai, H. J. Near-infrared fluorophores for biomedical imaging. *Nat. Biomed. Eng.* **1**, 0010 (2017).
52. Kenry, Duan, Y. K. & Liu, B. Recent advances of optical imaging in the second near-infrared window. *Adv. Mater.* **30**, 1802394 (2018).
53. Zhong, Y. T. et al. Boosting the down-shifting luminescence of rare-earth nanocrystals for biological imaging beyond 1500 nm. *Nat. Commun.* **8**, 737 (2017).
54. Zhang, H. X. et al. A mini-review on recent progress of new sensitizers for luminescence of lanthanide doped nanomaterials. *Nano Res.* **13**, 1795–1809 (2020).
55. Li, Y. B., Zeng, S. J. & Hao, J. H. Non-invasive optical guided tumor metastasis/vessel imaging by using lanthanide nanoprobe with enhanced down-shifting emission beyond 1500 nm. *ACS Nano* **13**, 248–259 (2019).
56. Wang, X. et al. Efficient erbium-sensitized core/shell nanocrystals for short wave infrared bioimaging. *Adv. Optical Mater.* **6**, 1800690 (2018).
57. Li, H. et al. Clearable shortwave-infrared-emitting NaErF₄ nanoparticles for noninvasive dynamic vascular imaging. *Chem. Mater.* **32**, 3365–3375 (2020).
58. Tan, M. L. et al. Rare-earth-doped fluoride nanoparticles with engineered long luminescence lifetime for time-gated in vivo optical imaging in the second biological window. *Nanoscale* **10**, 17771–17780 (2018).
59. Wang, W. et al. Er³⁺ self-sensitized nanoprobe with enhanced 1525 nm downshifting emission for NIR-IIb in vivo bio-imaging. *J. Mater. Chem. B* **9**, 2899–2908 (2021).
60. Deng, Z. M. et al. A high performance Sc-based nanoprobe for through-skull fluorescence imaging of brain vessels beyond 1500 nm. *Nanoscale* **10**, 9393–9400 (2018).
61. Liu, Z. et al. Boosting often overlooked long wavelength emissions of rare-earth nanoparticles for NIR-II fluorescence imaging of orthotopic glioblastoma. *Biomaterials* **219**, 119364 (2019).
62. Wang, Q. R. et al. Dye-sensitized rare earth-doped nanoparticles with boosted NIR-IIb emission for dynamic imaging of vascular network-related disorders. *ACS Appl. Mater. Interfaces* **13**, 29303–29312 (2021).
63. Ren, F. et al. Engineering NIR-IIb fluorescence of Er-based lanthanide nanoparticles for through-skull targeted imaging and imaging-guided surgery of orthotopic glioma. *Nano Today* **34**, 100905 (2020).
64. Song, D. et al. Sensitizing the luminescence of lanthanide-doped nanoparticles over 1500 nm for high-contrast and deep imaging of brain injury. *Anal. Chem.* **93**, 7949–7957 (2021).
65. Wang, T. et al. A hybrid erbium(III)-bacteriochlorin near-infrared probe for multiplexed biomedical imaging. *Nat. Mater.* **20**, 1571–1578 (2021).
66. Huang, J. H. et al. Enhanced efficiency of Er:Yb:Ce:NaGd(WO₄)₂ laser at 1.5–1.6 μm by the introduction of high-doping Ce³⁺ ions. *Opt. Lett.* **33**, 2548–2550 (2008).
67. Naczynski, D. J. et al. Rare-earth-doped biological composites as in vivo shortwave infrared reporters. *Nat. Commun.* **4**, 2199 (2013).
68. Zou, W. Q. et al. Broadband dye-sensitized upconversion of near-infrared light. *Nat. Photonics* **6**, 560–564 (2012).
69. Xue, B. et al. Ultrastrong absorption meets ultraweak absorption: unraveling the energy-dissipative routes for dye-sensitized upconversion luminescence. *J. Phys. Chem. Lett.* **9**, 4625–4631 (2018).
70. Zhang, X. B. et al. Boosting luminance energy transfer efficiency in upconversion nanoparticles with an energy-concentrating Zone. *Angew. Chem. Int. Ed.* **58**, 12117–12122 (2019).
71. Zhang, H. et al. Monitoring the opening and recovery of the blood–brain barrier with noninvasive molecular imaging by biodegradable ultrasmall Cu₂-Se nanoparticles. *Nano Lett.* **18**, 4985–4992 (2018).
72. Kim, J. et al. Recent progress of quantum dot-based photonic devices and systems: a comprehensive review of materials, devices, and applications. *Small Struct.* **2**, 2000024 (2021).
73. Bottrill, M., Kwok, L. & Long, N. J. Lanthanides in magnetic resonance imaging. *Chem. Soc. Rev.* **35**, 557–571 (2006).
74. Xing, H. Y. et al. A NaYbF₄:Tm³⁺ nanoprobe for CT and NIR-to-NIR fluorescent bimodal imaging. *Biomaterials* **33**, 5384–5393 (2012).
75. Jin, J. F. et al. Upconversion nanoparticles conjugated with Gd³⁺-DOTA and RGD for targeted dual-modality imaging of brain tumor xenografts. *Adv. Healthc. Mater.* **2**, 1501–1512 (2013).
76. Ni, D. L. et al. Dual-targeting upconversion nanoprobe across the blood–brain barrier for magnetic resonance/fluorescence imaging of intracranial glioblastoma. *ACS Nano* **8**, 1231–1242 (2014).
77. Ni, D. L. et al. Single Ho³⁺-doped upconversion nanoparticles for high-performance T₂-weighted brain tumor diagnosis and MR/UCL/CT multimodal imaging. *Adv. Funct. Mater.* **24**, 6613–6620 (2014).

78. Liu, Y. X. et al. Novel Cs-based upconversion nanoparticles as dual-modal CT and UCL imaging agents for chemo-photothermal synergistic therapy. *Theranostics* **6**, 1491–1505 (2016).
79. Dilmanian, F. A. et al. Response of rat intracranial 9L gliosarcoma to microbeam radiation therapy. *Neuro-Oncol.* **4**, 26–38 (2002).
80. Idris, N. M. et al. In vivo photodynamic therapy using upconversion nanoparticles as remote-controlled nanotransducers. *Nat. Med.* **18**, 1580–1585 (2012).
81. Park, Y. I. et al. Theranostic probe based on lanthanide-doped nanoparticles for simultaneous in vivo dual-modal imaging and photodynamic therapy. *Adv. Mater.* **24**, 5755–5761 (2012).
82. Stummer, W. et al. Fluorescence-guided surgery with 5-aminolevulinic acid for resection of malignant glioma: a randomised controlled multicentre phase III trial. *Lancet Oncol.* **7**, 392–401 (2006).
83. McNicholas, K., MacGregor, M. N. & Gleadle, J. M. In order for the light to shine so brightly, the darkness must be present—why do cancers fluoresce with 5-aminolaevulinic acid? *Br. J. Cancer* **121**, 631–639 (2019).
84. Rondags, A. et al. Fullerene C₆₀ with cytoprotective and cytotoxic potential: prospects as a novel treatment agent in Dermatology? *Exp. Dermatol.* **26**, 220–224 (2017).
85. Tzirakis, M. D. & Orfanopoulos, M. Radical reactions of fullerenes: from synthetic organic chemistry to materials science and biology. *Chem. Rev.* **113**, 5262–5321 (2013).
86. Wei, Z. et al. Engineered protein-Au bioplastic for efficient skin tumor therapy. *Adv. Mater.* **34**, 2110062, <https://doi.org/10.1002/adma.202110062> (2022).
87. Yu, Q. L. et al. Reductant-free synthesis of MnO₂ nanosheet-decorated hybrid nanoplatform for magnetic resonance imaging-monitored tumor micro-environment-responsive chemodynamic therapy and near-infrared-mediated photodynamic therapy. *Small Struct.* **2**, 2100116 (2021).
88. Sun, L. Y. et al. Creating structural defects of drug-free copper-containing layered double hydroxide nanoparticles to synergize photothermal/photodynamic/chemodynamic cancer therapy. *Small Struct.* **2**, 2000112 (2021).
89. Su, J. J. et al. Biocompatible inorganic nanoagent for efficient synergistic tumor treatment with augmented antitumor immunity. *Small* **18**, 2200897, <https://doi.org/10.1002/smll.202200897> (2022).
90. Liu, B. et al. Injectable and NIR-responsive DNA-inorganic hybrid hydrogels with outstanding photothermal therapy. *Adv. Mater.* **32**, 2004460 (2020).
91. Su, J. J. et al. Engineered protein photo-thermal hydrogels for outstanding in situ tongue cancer therapy. *Adv. Mater.* **33**, 2100619 (2021).
92. Zhou, T. et al. A dual mode nanophotonics concept for in situ activation of brain immune cells using a photoswitchable yolk-shell upconversion nanoformulation. *Nanomed.: Nanotechnol., Biol. Med.* **29**, 102279 (2020).
93. Liu, J. N. et al. Near-infrared voltage nanosensors enable real-time imaging of neuronal activities in mice and zebrafish. *J. Am. Chem. Soc.* **142**, 7858–7867 (2020).
94. Zhang, M. et al. Monitoring neuroinflammation with an HOCl-activatable and blood-brain barrier permeable upconversion nanoprobe. *Anal. Chem.* **92**, 5569–5576 (2020).
95. Ray, R. S. & Katyal, A. Myeloperoxidase: bridging the gap in neurodegeneration. *Neurosci. Biobehav. Rev.* **68**, 611–620 (2016).
96. Li, J. J. et al. Extracellular elastin molecule modulates Alzheimer's A β dynamics in vitro and in vivo by affecting microglial activities. *CCS Chem.* **3**, 1830–1837 (2021).
97. Li, Y. H. et al. Fluoro-substituted cyanine for reliable in vivo labelling of amyloid- β oligomers and neuroprotection against amyloid- β induced toxicity. *Chem. Sci.* **8**, 8279–8284 (2017).
98. Walkup, G. K. et al. A new cell-permeable fluorescent probe for Zn²⁺. *J. Am. Chem. Soc.* **122**, 5644–5645 (2000).
99. Peng, J. J. et al. High-efficiency in vitro and in vivo detection of Zn²⁺ by dye-assembled upconversion nanoparticles. *J. Am. Chem. Soc.* **137**, 2336–2342 (2015).
100. Kimura, E. et al. A macrocyclic zinc(II) fluorophore as a detector of apoptosis. *Proc. Natl Acad. Sci. USA* **100**, 3731–3736 (2003).
101. Maljevic, S. & Lerche, H. Potassium channels: a review of broadening therapeutic possibilities for neurological diseases. *J. Neurol.* **260**, 2201–2211 (2013).
102. Deisseroth, K. Optogenetics. *Nat. Methods* **8**, 26–29 (2011).
103. Chen, S. et al. Near-infrared deep brain stimulation via upconversion nanoparticle-mediated optogenetics. *Science* **359**, 679–684 (2018).
104. Zhang, F. et al. Optogenetic interrogation of neural circuits: technology for probing mammalian brain structures. *Nat. Protoc.* **5**, 439–456 (2010).
105. Deisseroth, K. & Anikeeva, P. Upconversion of light for use in optogenetic methods. *US patent* **9**, 522,288 (2011).
106. Hososhima, S. et al. Near-infrared (NIR) up-conversion optogenetics. *Sci. Rep.* **5**, 16533 (2015).
107. Shah, S. et al. Hybrid upconversion nanomaterials for optogenetic neuronal control. *Nanoscale* **7**, 16571–16577 (2015).
108. Wu, X. et al. Dye-sensitized core/active shell upconversion nanoparticles for optogenetics and bioimaging applications. *ACS Nano* **10**, 1060–1066 (2016).
109. Bansal, A. et al. Quasi-continuous wave near-infrared excitation of upconversion nanoparticles for optogenetic manipulation of *C. elegans*. *Small* **12**, 1732–1743 (2016).
110. Ai, X. Z. et al. Remote regulation of membrane channel activity by site-specific localization of lanthanide-doped upconversion nanocrystals. *Angew. Chem. Int. Ed.* **56**, 3031–3035 (2017).
111. Wang, Y. et al. Tetherless near-infrared control of brain activity in behaving animals using fully implantable upconversion microdevices. *Biomaterials* **142**, 136–148 (2017).
112. Lin, X. D. et al. Core-shell-shell upconversion nanoparticles with enhanced emission for wireless optogenetic inhibition. *Nano Lett.* **18**, 948–956 (2018).
113. Miyazaki, T. et al. Large timescale interrogation of neuronal function by fiberless optogenetics using lanthanide micro-particles. *Cell Rep.* **26**, 1033–1043.e5 (2019).
114. Terstappen, G. C. et al. Strategies for delivering therapeutics across the blood-brain barrier. *Nat. Rev. Drug Discov.* **20**, 362–383 (2021).